Study of collective ion acceleration in vacuum

W. W. Destler, H. S. Uhm, H. Kim, and M. P. Reiser

University of Maryland, College Park, Maryland 20742
(Received 21 September 1978; accepted for publication 10 November 1978)

Theoretical and experimental studies of the collective acceleration of ions by a linear electron beam in an evacuated drift tube are presented. A one-dimensional theoretical model of the collective acceleration process that predicts accelerated proton energies of many times the electron-beam energy is presented. The formation of a virtual cathode downstream of the anode-cathode gap is discussed, and the subsequent movement of the virtual cathode downstream as the anode plasma expands allows for enhanced acceleration of ions trapped in the potential well of the virtual cathode. Experiments reported indicate that effective electron beam propagation and effective collective acceleration occurs when a plasma source initially well confined to the anode is present.

PACS numbers: 29.15. − n, 52.60. + h

I. INTRODUCTION

In recent years, the collective acceleration of protons and heavier ions with linear (nonrotating) electron beams has been investigated at several laboratories.[1-16] Linear beam collective ion acceleration of ions by the interaction of an intense electron beam with a neutral gas background was first reported by Graybill *et al.*[1] and experimental and theoretical work in this area has continued at several laboratories.[2-8] The acceleration of ions in vacuum, where the positive ions are provided by an insulating anode material, was first reported by Luce,[9] and further studies of this phenomenon have been conducted by researchers at Maryland,[10-12] Cornell,[13] Kirtland Air Force Base, [14,15] and Boeing.[16] In these experiments, a relativistic electron beam is injected through an axial hole in a dielectric anode. The diode and downstream drift tube are evacuated to 10^{-5} Torr or better and accelerated ions are typically detected using nuclear activation techniques. Collectively accelerated protons have been observed in these systems with energies of up to 20 times the electron-beam energy, and heavier ions (C, N, O, F, and Cl) have been accelerated to energies of several MeV per nucleon. The accelerated ion energies observed in these experiments are consistently greater than those observed when electron beams of similar current and energy are injected into a neutral gas background.

Several theoretical models have been proposed to explain this acceleration process. The formation of a virtual cathode downstream of the anode was predicted by Poukey and Rostoker[17] to occur when the injected electron-beam current exceeds the limiting current for propagation of an electron beam of radius a in a grounded cylinder of radius R. This limiting current is given by

$$I_l = \frac{17\,000(\gamma_0^{2/3} - 1)^{3/2}}{[1 + 2\ln(R/a)](1 - f)} \quad \text{(A)}, \tag{1}$$

where γ_0 is the relativistic mass factor for the electrons after acceleration in the anode-cathode gap and f is the ratio of the ion density to the electron density. The transient overshoot of the depth of the potential well associated with the virtual cathode to values of two to three times the peak electron energy and the subsequent collapse and movement of the virtual cathode when ions are introduced have been used by Olson[7] to explain the collective acceleration of ions in a neutral gas background. The ion energies observed in the evacuated systems, however, are too high to be explained solely on this basis, and several possible mechanisms have been advanced in an effort to explain the favorable experimental results. Boyer, Kim, and Zorn[10] suggested that in these systems the early part of the electron beam forms a dense plasma that is initially well confined to the anode region. The subsequent diffusion of this plasma into the downstream region should allow a movement of the virtual cathode downstream, and enhanced acceleration may be expected of those ions that are trapped and accelerated by the electric fields associated with the moving potential well. A one-dimensional description of this process is given in Sec. II.

Zucker *et al.*[18] has proposed that, during the electron-beam pulse, this dielectric anode disk becomes a microwave cavity resonator excited by surface flashover currents. He suggests that very high electric field gradients in the anode hole may accelerate the ions. In addition, Luce *et al.*[19] have suggested that some of the acceleration effects may be attrributable to dense plasma vortex filaments.

Recent experiments have added important information on the acceleration process. Hoeberling *et al.*[14] demonstrated experimentally that the acceleration process is critically dependent upon the ratio of the electron-beam current to the limiting current. In particular, this work showed that effective collective acceleration is not observed for $I/I_l < 1$. The electron-beam propagation characteristics under these conditions were not reported.

Boyer *et al.*[11] demonstrated the critical relationship between the effectiveness of collective ion acceleration in such systems and the total electron-beam power, even when the current is maintained well above the limiting current for a given configuration. Experimental results by Destler and Kim[12] have indicated that the acceleration of heavy ions (C, F, O, and N) in these systems may be enhanced by preforming a plasma in the anode region using the electron-beam accelerator prepulse.

 0021-8979/79/053015-08$01.10

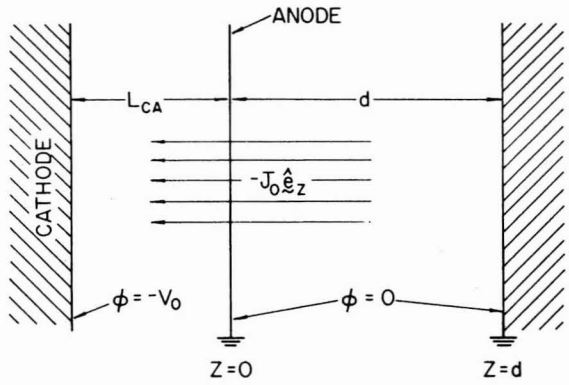

FIG. 1. Grounded plane conductors with cathode and anode.

Several schemes have been shown experimentally to result in an enhancement of the accelerated ion energy by exercising some control over the electron-beam propagation in the region downstream of the anode. These include systems of lenses,[9] floating electrodes,[10,11] and a helical slow-wave structure.[11,20] In a related experiment, Olson[21] has shown that the electron-beam-front propagation may be controlled by laser ionization of a background gas (the ionization front accelerator scheme).

A major difference between collective acceleration in vacuum and collective acceleration in a neutral gas background is that the source of ions in the first case is initially well confined to the region of the anode. In a related experiment, Olson *et al.*[22] used a laser to enhance the production of ions from an aluminum anode foil through which an intense electron beam was fired. While the acceleration of highly stripped aluminum ions was not observed, the laser did appear to enhance the acceleration of impurities contained on the anode surface.

In this paper, theoretical and experimental studies of the collective acceleration of ions in vacuum are reported. A one-dimensional theoretical model of the electron-beam propagation and the collective acceleration process is proposed and described in Sec. II. Experimental studies of the electron-beam propagation characteristics, both with and without the fractional neutralization provided by ions, and the relationship between the electron-beam propagation and the collective acceleration of ions are presented in Sec. III. Conclusions are drawn in Sec. IV.

II. ONE-DIMENSIONAL THEORY

A. Steady-state equilibrium for an electron beam propagating between two plane conducting boundaries

The case of an electron beam propagating away from a single-plane conducting boundary has been treated previously.[17] In Sec. II, the steady-state equilibrium properties of a relativistic non-neutral electron beam propagating between two grounded plane conductors are investigated. The general configuration under consideration is shown in Fig. 1. Two grounded infinite plane conductors are located at $z = 0$ and $z = d$, and a relativistic non-neutral electron beam is injected through the conductor at $z = 0$ with current density $\mathbf{J}_i = -J_0\hat{e}_z$. Here, $\hat{e}_z$ is a unit vector along the z direction. The distance between the conductor at $z = 0$ (anode) and the cathode with electric potential $\phi = -V_0$ is denoted by L_{CA}. Since the conductors are assumed to be infinite planes, the influence of self-magnetic fields is neglected throughout this description. In this context, the analysis is reduced to a one-dimensional problem.

The steady-state Poisson equation for the space-charge fields in the region between the two plane conductors is

$$\frac{\partial^2\phi(z)}{\partial z^2} = -\frac{\rho(z)}{\epsilon_0}, \tag{2}$$

where $\phi(z)$ is the electrostatic potential, ϵ_0 is the permittivity of free space, and the charge density $\rho(z)$ is defined by

$$\rho(z) = J(z)/\beta(z)c. \tag{3}$$

Here, $J(z)$ and $\beta(z)$ are the current density and electron speed, respectively, at axial coordinate z. The boundary conditions for Eq. (2) are

$$\phi(z=0) = \phi(z=d) = 0. \tag{4}$$

For notational convenience, we define

$$\gamma_0 = (1-\beta_0^2)^{-1/2} = 1 + eV_0/mc^2,$$
$$\gamma(z) = [1-\beta(z)^2]^{-1/2} = 1 + e[V_0 + \phi(z)]/mc^2. \tag{5}$$

The analysis of the steady-state Poisson equation (2) can be separated into two cases. In the first case, the injection current density J_0 is sufficiently small that all of the electrons in the injected beam reach the plane conductor at $z = d$. In this case, $J(z) = -J_0$ and substituting Eqs. (3) and (5) into Eq. (2) yields

$$\frac{\partial^2\gamma}{\partial z^2} = \frac{eJ_0}{mc^3\epsilon_0}\frac{\gamma}{(\gamma^2-1)^{1/2}}. \tag{6}$$

The remaining boundary conditions for Eq. (5) are

$$\left(\frac{\partial\gamma}{\partial z}\right)_{z=d_m} = \left(\frac{\partial\phi}{\partial z}\right)_{z=d_m} = 0, \tag{7}$$

where d_m represents the position of the minimum potential ϕ_m, i.e., $\phi(z=d_m) = \phi_m$. Integrating Eq. (6) twice and making use of Eqs. (4) and (7), we obtain

$$F(\gamma_0,\gamma_m) = \left(\frac{2eJ_0}{mc^3\epsilon_0}\right)^{1/2} d_m, \quad z < d_m,$$

$$= \left(\frac{2eJ_0}{mc^3\epsilon_0}\right)^{1/2} (d-d_m), \quad z > d_m,$$

where

$$F(\gamma_0,\gamma_m) = \int_{\gamma_m}^{\gamma_0} d\gamma[(\gamma^2-1)^{1/2} - (\gamma_m^2-1)^{1/2}]^{-1/2}, \tag{9}$$

where $\gamma_m = 1 + e[(V_0+\phi_m)/mc^2]$ is the relativistic mass factor for the electrons at $z = d_m$. It is evident from Eq. (8) that the value of d_m corresponding to the minimum potential is given by

$$d_m = \tfrac{1}{2}d. \tag{10}$$

Substituting Eq. (10) into Eq. (8), we obtain the equation of

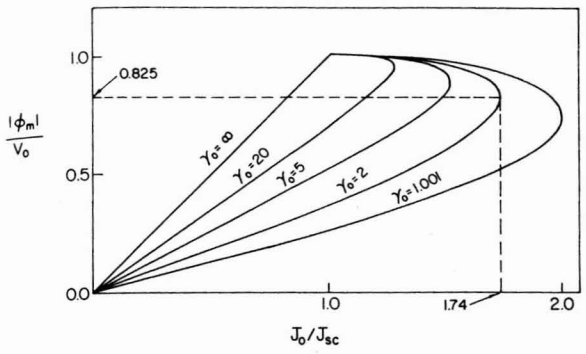

FIG. 2. Characteristic curves [Eq. (11)] for two plane conductors are presented for several values of γ_0.

the characteristic curve for a relativistic electron beam propagating between two plane conductors

$$J_0 = \frac{2mc^2\epsilon_0}{ed^2} F(\gamma_0,\gamma_m)^2, \tag{11}$$

which relates the injection current intensity J_0 and the minimum potential ϕ_m for specified γ_0 and d. This result was first obtained by Voronin *et al.*[23]

As a check on the relation given in Eq. (11), it is instructive to consider the case $\phi_m = -V_0$. Equation (11) can then be expressed as

$$J_{SC} = J_0(\gamma_m = 1) = \frac{mc^3\epsilon_0}{2e(\frac{1}{2}d)^2}\left(\int_1^{\gamma_0}\frac{d\gamma}{[\gamma^2-1)^{1/4}]}\right)^2, \tag{12}$$

which is the space-charge-limited current density. Equation (12) is identical to the relativistic Child law obtained by Jory and Trivelpiece[24] for an effective cathode-anode distance equal to $\frac{1}{2}d$.

In order to illustrate the influence of the injection current density on the space-charge field, characteristic curves obtained from Eq. (11) are presented in Fig. 2, where the absolute value of normalized minimum potential $|\phi_m|/V_0$ is plotted versus J_0/J_{SC} for several values of γ_0. Several points are noteworthy in Fig. 2. First, for specified γ_0, static solutions for ϕ_m/V_0 exist only when J_0 is smaller than the critical value $J_C(\gamma_0)$ corresponding to the allowable maximum value of J_0. Defining the critical potential $\phi_C(\gamma_0) = \phi_m(J_0 = J_C)$, we obtain

$$J_C = \frac{2mc^3\epsilon_0}{ed^2} F(\gamma_0,\gamma_C)^2, \tag{13}$$

where $\gamma_C = 1 + e(V_0 + \phi_C)/mc^2$. For example, for $\gamma_0 = 2$, the critical value of current density is $J_C = 1.74J_{SC}$, and $\phi_C(V_0 = 2) = -0.825V_0$. Second, for the range $0 < J_0 < J_{SC}$, $\phi_m(J_0)$ is a single-valued function of J_0. On the other hand, when $J_{SC} < J_0 < J_C$, we obtain two different values of $|\phi_m|$ for a given J_0. However, only the smaller of these two values is a stable and physically attainable solution. The other solution is unstable. For example, for $\gamma_0 = 2$ and $J_0 = 1.5J_{SC}$, the solution $|\phi_m| = 0.6V_0$ is stable, whereas $|\phi_m| = 0.96V_0$ is unstable. In this context, it is evident that the condition $\phi_m = -V_0$ and $J_0 = J_{SC}$ can never be reached for a steady-state equilibrium. Third, for $\gamma_0 \to \infty$, ϕ_m is linearly proportional to J_0, i.e., $\phi_m = -V_0 J_0/J_{SC}$ for $0 < J_0 < J_{SC}$.

When the injection current intensity J_0 exceeds the critical current density J_C, excess charge will accumulate in the region of the potential minimum until $\phi_m = -V_0$, at which time a portion of the injected beam will be reflected back toward the anode at $z = 0$. Since there is no steady-state solution $\phi_m(J_0)$ for $J_0 > J_C$, as shown in Fig. 2, it is evident that the absolute value of the minimum potential $|\phi_m|$ will increase from $|\phi_C|$ to V_0 within a few multiples of the electron transit time between the two plane conductors. The process leading to the state $\phi_m = -V_0$ is nonadiabatic, and $|\phi_m|$ can be temporarily larger than V_0, eventually oscillating about the point $\phi_m = -V_0$. In a similar manner, it is expected that the position of the potential minimum will also oscillate about $z = d_m$. This oscillation, however, can be easily eliminated by introducing a small amount of energy spread (see Sec. II B).

In order to determine the time-averaged properties of the system for $J_0 > J_C$, we assume that a virtual cathode with $\phi_m = -V_0$ is formed at $z = d_m$. Allowing for a return current, it is evident that the charge density can be expressed as

$$\rho(z) = -pJ_0/\beta(z)c, \quad z > d_m, \qquad = (p-2)J_0/\beta(z)c, \quad z < d_m, \tag{14}$$

where p and d_m will be determined by the parameters J_0 and γ_0 [Eqs. (17) and (18)]. As shown in Fig. 1, the injection current intensity J_0 in Eq. (14) will be equal to the space-charge-limited current density in the anode-cathode region. Therefore, from Eq. (12), J_0 can be expressed as

$$J_0 = J_{CA} = \frac{mc^3\epsilon_0}{2eL_{CA}^2}\left(\int_1^{\gamma_0}\frac{d\gamma}{(\gamma^2-1)^{1/4}}\right)^2, \tag{15}$$

where L_{CA} is the cathode-anode distance.

Substituting Eq. (14) into Eq. (1) and carrying out the integration, we obtain

$$L_{CA}^2 = p(d-d_m)^2, \quad z > d_m \qquad = (2-p)d_m^2, \quad z < d_m, \tag{16}$$

where use has been made of Eqs. (4) and (15), and the condition $\phi(z = d_m) = -V_0$. Straightforward algebraic manipulation yields

$$\frac{2d_m}{d} = 1 - \left[1 + 2\left(\frac{L_{CA}}{d}\right)^2 - 2\left(\frac{L_{CA}}{d}\right)\left(2 + \frac{L_{CA}^2}{d^2}\right)^{1/2}\right]^{1/2} \tag{17}$$

and

$$p = \frac{L_{CA}^2}{(d-d_m)^2}. \tag{18}$$

The cathode-anode distance L_{CA} can be expressed in terms of J_0 and γ_0, as can the parameters d_m and p [Eqs. (15), (17), and (18)].

To investigate collective ion acceleration, it is important to determine the electric field intensity E_0 at the downstream surface of the anode. Substituting Eq. (14) into Eq. (2) and making use of the condition $\phi(z=d_m)=-V_0$ yields

$$E_0=\left(\frac{2mc(2-p)J_0}{e\epsilon_0}\right)^{1/2}(\gamma_0^2-1)^{1/4}. \tag{19}$$

Similarly, the electric field intensity E_{CA} at the upstream surface of the anode is given by

$$E_{CA}=\left(\frac{2mcJ_0}{e\epsilon_0}\right)^{1/2}(\gamma_0^2-1)^{1/4}.$$

Substituting this result into Eq. (19), we obtain

$$E_0=(2-p)^{1/2}E_{CA}, \tag{20}$$

where the parameter p [see Eq. (18)] satisfies $p\leq 1$. Thus, the electric field intensity at the downstream surface of the anode is always greater than the electric field intensity at the upstream surface of the anode.

When the distance d between the two plane conductors is much greater than the cathode-anode distance, i.e., $d \gg L_{CA}$, Eqs. (17) and (18) can be approximated by

$$d_m \cong L_{CA}/1.414 \tag{21}$$

and

$$p \cong L_{CA}^2/d^2 \cong 0. \tag{22}$$

It should be noted from Eq. (21) that the virtual cathode-anode distance d_m is smaller than the actual cathode-anode distance L_{CA}. Moreover, almost no forward current propagates beyond $z=d_m$. Substituting Eq. (22) into Eq. (19), we obtain

$$E_0=\left(\frac{4mcJ_0}{e\epsilon_0}\right)^{1/2}(\gamma_0^2-1)^{1/4} \tag{23}$$

for $d \gg L_{CA}$. The electric field intensity in Eq. (23) can be used to accelerate ions in the region between two plane conductors.

B. Space-charge effects of a pulsed electron beam

The space-charge effects of a pulsed electron beam with $J_0 > J_C$ are investigated in this section, including the influence of a return current. A one-dimensional model is used as in Sec. II A, and the effects of self-magnetic-fields are again neglected. The electron beam is injected through the anode into the region between the two plane conductors shown in Fig. 1. The subsequent temporal and spatial evolution of the beam are studied by computer simulation with the time measured in units of the free-electron transit time between the cathode and the anode

$$\tau = L_{CA}/\beta_0 c.$$

For notational convenience in the subsequent analysis, we express the normalized injection current intensity J_0/J_{SC} as

$$\frac{J_0}{J_{SC}}=\left(\frac{d}{2L_{CA}}\right)^2, \tag{24}$$

where use has been made of Eqs. (12) and (15).

A one-dimensional simulation code has been developed to investigate the properties of a pulsed beam propagating between two plane conductors. Negatively charged plane layers are injected into the system at equal time intervals. The Poisson equation is solved self-consistently at each time interval to determine the electric force exerted on the charged layers, thereby calculating the equation of motion for each layer. Approximately 300 layers are admitted into the system during the computer simulation.

In order to illustrate the influence of an axial energy spread on the oscillations observed for beams with $J_0 > J_C$, we assume in the one-dimensional model that the transverse energy spread is negligible and that injected electron energy distribution is given by

$$f(\gamma_0)=(J_0/\Delta)U[\Delta^2-4(\gamma_0-\hat{\gamma}_0)^2], \tag{25}$$

where $\gamma_0 m$ is the initial relativistic electron mass for a particular electron, $\hat{\gamma}_0 m$ is its mean value, and U is the Heaviside step function defined by

$$U(x)=0, \quad x<0$$
$$U(x)=1, \quad x>0.$$

Equation (25) is normalized to give

$$J_0=\int_1^\infty d\gamma_0 f(\gamma_0).$$

It is evident from Eq. (25) that Δ is a measure of the total energy spread.

Typical simulation results are shown in Fig. 3. Since we are interested in applications of this theory to collective ion acceleration, the space-charge effects of a relativistic rectangular-shaped pulsed beam for $d \gg L_{CA}$ are investigated. Shown in Fig. 3 are temporal plots of (a) the normalized electric field intensity $E_0 L_{CA}/V_0$ at the right-hand surface of the anode, (b) the normalized minimum potential ϕ_m/V_0, and (c) the minimum potential position d_m/d for the conditions $\gamma_0=5$, $\alpha=\Delta/(\hat{\gamma}_0-1)=0$, and $d/L_{CA}=20$ corresponding to $J_0=100J_{SC}$ [see Eq. (24)]. It is evident from Fig. 3 that the magnitude of the minimum potential $|\phi_m|$ assumes a large value ($|\phi_m| \approx 2V_0$) at the beginning of the beam pulse ($t \approx 4\tau$), which is consistent with the result obtained by Poukey and Rostoker.[17] At later times, however, the quantities E_0, ϕ_m, and d_m oscillate about the static equilibrium values given in Eqs. (17)–(19). The virtual cathode formed at $d_m \approx L_{CA}$ permits essentially no forward current. We also note from Fig. 3(a) that the average intensity of the electric field at the right-hand surface of the anode is given by approximately $2V_0/L_{CA}$, which may be used to accelerate the ions in a plasma located at the anode.

It is interesting to note that the average magnitude of the minimum potential $|\phi_m|$ is increased by increasing the energy spread. Figure 4 shows a plot of ϕ_m/V_0 versus t/τ for $\alpha=\Delta/(\hat{\gamma}_0-1)=0.375$ and parameters otherwise identical to those used above (Fig. 3). It is evident from Fig. 4 that the average value of $|\phi_m|=1.2V_0$, which is considerably larger than the value $|\phi_m|=V_0$ indicated in Fig. 3(b). Moreover, the oscillation amplitude is significantly reduced by the energy spread.

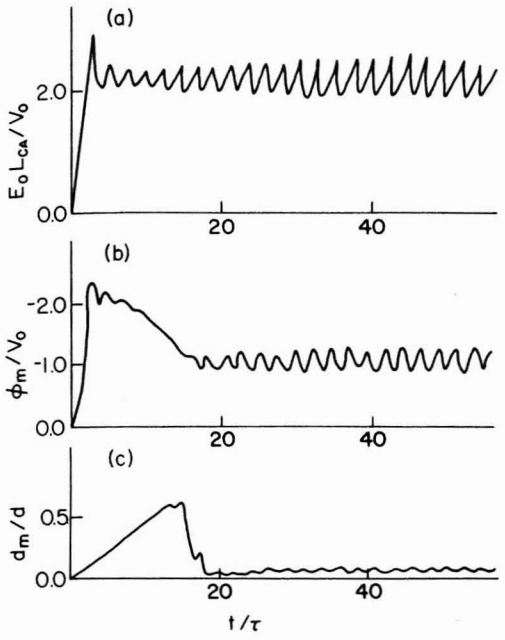

FIG. 3. Time evolution of (a) normalized electric field intensity $E_0 L_{CA}/V_0$ at the downstream surface of the anode, (b) normalized minimum potential ϕ_m/V_0, and (c) minimum potential position d_m/d for $\gamma_0 = 5$ and $d/L_{CA} = 20$ corresponding to $J_0 = 100\, J_{SC}$. No energy spread.

C. A model of collective ion acceleration in vacuum

Mechanisms for collective ion acceleration by intense electron beams have been proposed by Poukey and Rostoker[17] and Olson,[7] which utilize the initial overshooting of the minimum potential ϕ_m and its subsequent damping by ionization processes, while positive ions are accelerated [see Fig. 3(b) for $t \lesssim 10\tau$]. In this section we present a possible mechanism for collective ion acceleration that may be viewed as similar to an ambipolar diffusion process. The early portion of the electron beam is assumed to produce a dense neutralized plasma at the anode plane (although in principle the plasma might be created by external means as well). The high-energy electrons make a virtual cathode with the minimum potential located just outside the plasma boundary. A large electric field with intensity E_0 given in Eq. (23) is created near the plasma surface, accelerating positive ions toward the virtual cathode. The ions neutralize the space charge produced by the electron beam, thereby expanding the plasma boundary. In this context, the virtual cathode moves coherently with the positive ions.

To make analysis tractable, we assume that the accelerated ions form a layer with surface mass density

$$\sigma = \epsilon_0 E_0 M/Ze, \tag{26}$$

where E_0 is given by Eq. (23) and Z and M are the ion charge state and the rest mass, respectively. If we identify the ion layer as a piston wall and the electrons as particles inside the piston, it is straightforward to show that the momentum gain Δp of the ion layer, produced by an individual electron collision, can be expressed as

$$\Delta p = 2\gamma_0 m(v_e - v_i), \tag{27}$$

where v_i is the ion speed, v_e and $\gamma_0 m$ are the electron speed and mass, respectively, at the plasma surface. To obtain Eq. (27), we have assumed that the ion motion is nonrelativistic.

Since the electron flux is given by $n_e(v_e - v_i)m$ we obtain

$$\frac{d}{dt}(\sigma v_i) = 2\gamma_0 m n_e (v_e - v_i)^2, \tag{28}$$

where use has been made of Eq. (27). Here, n_e is the electron density at the plasma surface. Substituting Eqs. (23) and (26) into Eq. (28) and integrating yields

$$v_i(t) = v_e\left\{1 - \left[1 + Z(t - t_0)\frac{\gamma_0 m}{M} \times \left(\frac{eJ_0}{mc\epsilon_0}\right)^{1/2}(\gamma_0^2 - 1)^{-1/4}\right]^{-1}\right\}, \tag{29}$$

where use has been made of the identity $J_0 = en_e v_e$ and the initial condition $v_i(t = t_0) = 0$. For $v_i(t) \ll c$, the mean ion kinetic energy is given by

$$\bar{W}_K = \tfrac{1}{2} M v_i(t)^2. \tag{30}$$

It is evident from Eq. (29) that the ion kinetic energy is increased by prolonging the acceleration time $\Delta t = t - t_0$. The injection current intensity J_0 and the beam energy γ_0 also play very important roles in increasing the ion kinetic energy. As an example, consider an electron beam with $\gamma_0 = 2$ and injection current intensity $J_0 = 13$ kA/cm^2. In this case, the mean proton kinetic energy is $\bar{W}_K = 6$ MeV for $\Delta t = 2$ nsec and $\bar{W}_K = 20$ MeV for $\Delta t = 4$ nsec. According to the one-dimensional model, considerably higher ion energies can be obtained as a result of this process. In actual experiments, however, the electron beam is usually injected through a hole in the anode of about 1 cm diameter. When the resultant anode plasma surface expands more than 1 cm downstream, the applicability of this one-dimensional model becomes doubtful since the electric field associated with the virtual cathode will becomes progressively weaker as the plasma expands away from the anode.

A two-dimensional model would show that the virtual cathode is formed when the injected current exceeds the limiting current given in Eq. (1), but the coherent movement of the virtual cathode along with the ions, leading to acceler-

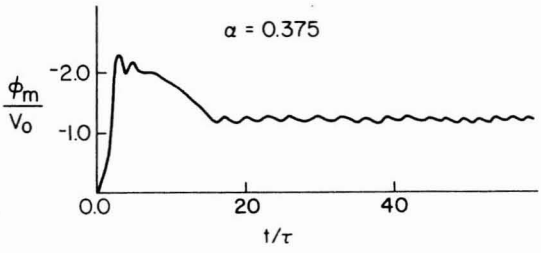

FIG. 4. Plot of normalized minimum potential ϕ_m/V_0 versus t/τ for energy spread $\alpha = \Delta/(\gamma_0 - 1) = 0.375$ and parameters otherwise identical to Fig. 3.

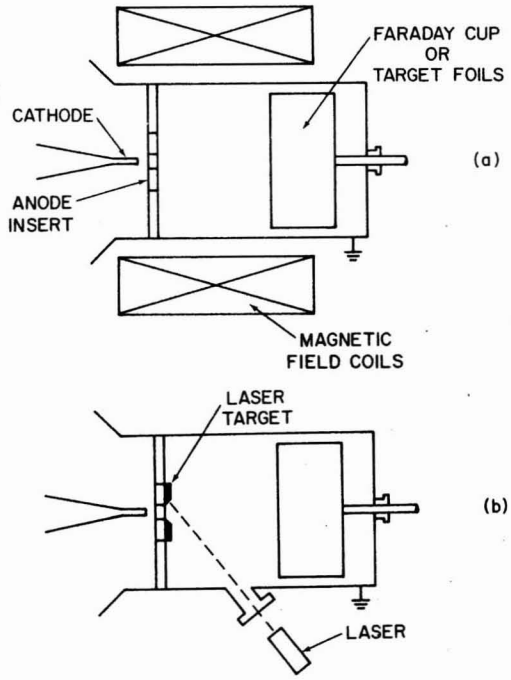

FIG. 5. Experimental configurations.

ated ion energies substantially in excess of that predicted by the depth of the virtual cathode potential well alone, should be quite similar to the process described one dimensionally above. It is important to note that this process does not require that ϕ_m be greater than V_0 in order to explain the high ion energies observed experimentally.

III. EXPERIMENTS

The general experimental configuration is shown in Fig. 5(a). An intense relativistic electron-beam pulse (1.5 MV, 35 kA, 30 nsec FWHM) is emitted from a tungsten needle cathode located 6–7 mm in front of the anode plane. The anode is a thick conducting disk into which a 5-cm-diam anode insert may be inserted coaxially. The anode-insert material may be either conducting (usually stainless steel) or insulating (polyethylene, Teflon, etc.) and has an 11-mm-hole bored in it on axis to allow most of the electron beam to pass through the anode plane into the acceleration region. The downstream drift tube is 30 cm in diameter, and a system of magnetic field coils powered by a 100-kW dc power supply is available to apply up to 3 kG to the electron-beam drift region.

Diagnostics for measuring the electron-beam propagation characteristics include voltage and current monitors near the cathode position and a 15-cm-diam movable Faraday cup inserted from the downstream end of the vacuum chamber. Accelerated ions are detected by foil activation techniques, using copper or aluminum target foils. Neutron-producing reactions are detected using a silver activation neutron detector located at the target position 90° from the system axis. All experiments were performed in a vacuum upstream and downstream of the anode of about 5×10^{-5} Torr.

A. Electron-beam propagation in the absence of ions

With a stainless-steel disk inserted into the anode, the electron-beam current has been measured as a function of axial position downstream of the anode plane. A movable Faraday cup was used to measure the current and results are shown in Fig. 6(a) for three different values of applied magnetic field. It is easily seen that the measured electron-beam current falls off rapidly as the Faraday cup is moved away from the anode plane. Since the Faraday cup is a very-low-impedance shunt ($3\times10^{-3}\ \Omega$), the device acts as a relatively large perturbation to the boundary conditions seen by the electron beam for axial positions close to the anode. It is likely, therefore, that the actual electron-beam current falls even more rapidly than is observed by this measurement technique. Nevertheless, the measurements indicate clearly that beam current in excess of the limiting current (calculated by assuming that $f=0$ and that the beam diameter is given by the anode-insert hole diameter) is not observed to propagate away from the anode region. The limiting current for these conditions is also indicated in Fig. 6.

B. Electron-beam propagation with ions

The electron-beam propagation characteristics in the presence of ions have been measured by two different techniques. In the first set of experiments, the stainless-steel an-

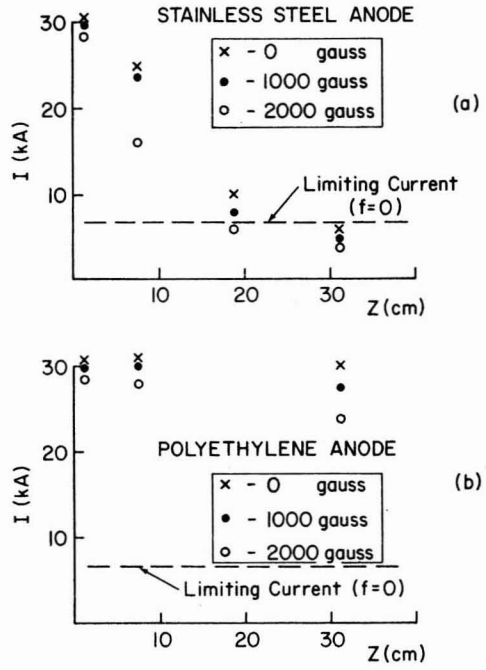

FIG. 6. Peak electron-beam current measured as a function of axial position for (a) a conducting metallic anode and (b) an insulating dielectric anode.

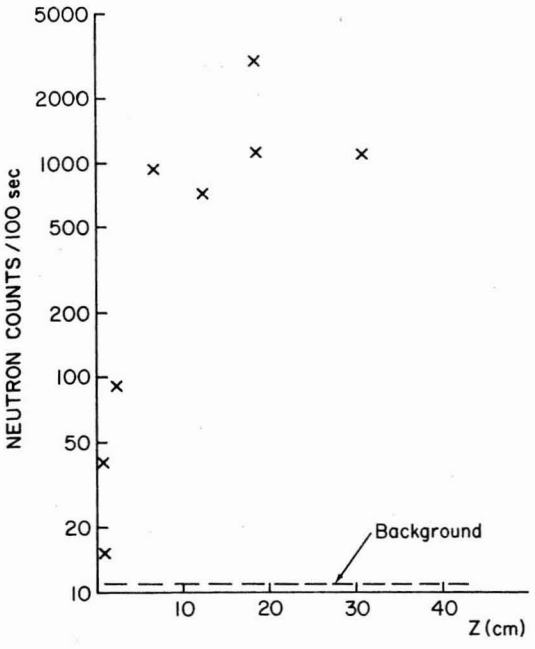

FIG. 7. Relative neutron production from ions striking target foils as a function of the axial position of the target.

ode was replaced by a polyethylene anode insert of the type used for proton acceleration in a standard Luce diode. Measurements of the electron-beam current as a function of axial position downstream of the anode plane are shown in Fig. 6(b) and indicate clearly that under these conditions the full electron-beam current propagates to the end of the drift tube. The mean electron-beam velocity under these conditions is measured to be less than $0.1c$, an indication that the electron-beam propagation is controlled by the expansion of the plasma produced at the anode by electron bombardment and surface breakdown.

Accelerated protons under these conditions have been detected using nuclear activation of copper foils [$Cu^{63}(p,n)Zn^{63}$ and $Cu^{65}(p,n)Zn^{65}$]. The neutrons produced from these reactions have been measured as a function of axial position using a movable target holder inserted from the downstream end of the vacuum chamber. The target mount was designed to allow the copper target to effectively float from ground in order to minimize the perturbation to the boundary conditions seen by the beam as the target is moved close to the anode plane. Results of these measurements are shown in Fig. 7 for the case $B = 0$. It is easily seen that neutron production, and presumably accelerated ion energy and current, does not significantly increase when the target is moved further than 6 cm away from the anode plane. Measurements of the activation of stacked copper foils from the reaction $Cu^{63}(p,n)Zn^{63}$ indicate that the peak observed proton energy in this case is about 8 MeV. It is important to note that this peak proton energy is clearly in excess of that inferred from the mean electron-beam propagation velocity.

An independent measurement of the role the ions play in the electron-beam transport process has been obtained from the experiment shown schematically in Fig. 5(b). A stainless-steel anode insert is used, and a preformed laser-produced plasma is independently generated on the downstream side of the anode. The plasma is generated using a carbon target and a 0.8-J 30-nsec Q-switched ruby laser fired at the target through a vacuum window at an angle of 45° to the system axis. The delay between the laser firing time τ_L and the electron-beam firing time τ_B may be varied over a wide range. Eventually, the independent preparation of electron beam and ion source should allow greatly improved ion-beam quality and reproducibility, although the modest laser power available in these experiments was not sufficient to achieve optimum results. Measurements of the electron-beam current propagating to the end of the drift tube as a function of the firing delay $\tau_L - \tau_B$ are shown in Fig. 8(a). The delay time of several μsec for optimum beam propagation is sufficient to allow the laser-produced plasma to expand to a few times the beam radius before the electron beam arrives. Note that at no time is the full available electron-beam current of 30 kA able to propagate to the end of the drift tube. This result is attributed to the modest laser energy available. It is likely that insufficient plasma is produced to allow full electron-beam propagation. Measurements of the neutrons produced when accelerated ions strike aluminum target foils located at the end of the drift tube are shown in Fig. 8(b) and clearly show that the collective acceleration is observed only when electron-beam propagation is allowed by the plasma ions. The neutrons produced are possibly at-

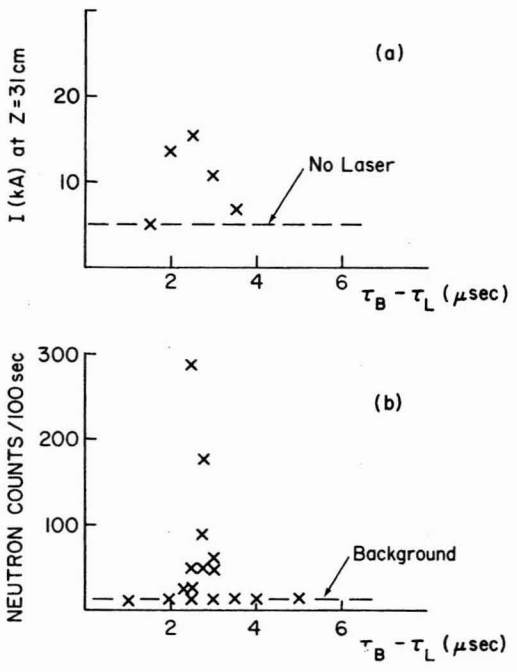

FIG. 8. (a) Peak electron-beam current propagating to the end of the drif tube and (b) relative neutron production from ions striking target foils as a function of the delay between laser firing and electron-beam pulse arrival.

tributable to the reaction $Al^{27}(C^{12},C^{12}n)Al^{26}$, which has a threshold of about 19 MeV. In addition, the reaction $Al^{27}(C^{12},C^{11})Al^{28}$ has been detected from both the γ-ray energies and the product half-lives. From considerations of both the Coulomb barrier and the cross section for this reaction, the probable carbon-ion energy is estimated to be at least 20 MeV.

IV. CONCLUSIONS

In this paper, theoretical and experimental studies of the collective acceleration of ions in vacuum have been presented. The most important conclusions to be drawn from this work are as follows:

(1) The one-dimensional theoretical model presented in Sec. II indicates that when an intense relativistic electron beam is injected into a drift region downstream of the anode, electron-beam current in excess of the space-charge-limiting current will not be observed unless space-charge neutralization is provided by background ions diffusing downstream from the anode. The experimental results presented in Sec. III confirm this result.

(2) The "piston model" mechanism proposed in an attempt to explain the high accelerated ion energies observed in these systems does not rely on the overshoot of the depth of the potential well associated with the virtual cathode to values in excess of the peak anode-cathode potential. It does rely upon an ion source initially well confined to the anode that allows the virtual cathode to move coherently away from the anode as ions are being accelerated.

(3) The effective acceleration of ions in the case when a conducting anode is used in place of a dielectric anode and ions are produced independently by laser-target interaction is a strong indication that dielectric anodes in such systems serve simply as a source of ions initially well confined to the anode region.

(4) The independent preparation of electron beam and ion source should eventually allow for better system optimization and reproducibility.

ACKNOWLEDGMENTS

It is a pleasure to acknowledge the benefit of useful discussions with Dr. Ronald C. Davidson. Experimental assistance was provided by Dr. W. Namkung. This work was supported by the National Science Foundation. The research of one of the authors (HSU) was supported in part by the Office of Naval Research under the auspices of the University of Maryland–Naval Research Laboratory Joint Program in Plasma Physics.

[1]S.E. Graybill and J.R. Uglum, J. Appl. Phys. **41**, 236 (1970).
[2]J. Rander, Phys. Rev. Lett. **25**, 893 (1970).
[3]G.W. Kuswa, Ann. N.Y. Acad. Sci. **25**, 514 (1975).
[4]D. Ecker and S. Putnam, IEEE Trans. Nucl. Sci. **NS-20**, 305 (1973).
[5]D.C. Straw and R.B. Miller, Appl. Phys. Lett. **25**, 379 (1974).
[6]A.A. Kolomensky, Proc. IXth Int. Accel. Conf. High Energy Accel., SLAC, 1974, p. 254 (unpublished).
[7]C.L. Olson, Phys. Fluids **18**, 585 (1975).
[8]S. Graybill and F. Young, Bull. Am. Phys. Soc. **21**, 1058 (1976).
[9]J.S. Luce, Ann. N.Y. Acad. Sci. **25**, 2171 (1975).
[10]C.N. Boyer, H. Kim, and G.T. Zorn, Proc. Int. Topical Conf. on Electron Beam Res. and Tech., Albuquerque, N.M., 1975, Vol. II (unpublished).
[11]C.N. Boyer, W.W. Destler, and H. Kim, IEE Trans. Nucl. Sci. **NS-24**, 1625 (1977).
[12]W.W. Destler and H. Kim, Proc. 2nd Int. Topical Conf. on High Power Electron and Ion Beam Res. and Tech., Ithaca, N.Y., 1977, p. 521 (unpublished).
[13]R. Williams, J.A. Nation, and M.E. Read, Bull. Am. Phys. Soc. **21**, 1059 (1976).
[14]R.F. Hoeberling and D.N. Payton III, J. Appl. Phys. **48**, 2079 (1977).
[15]R.B. Miller and R.J. Faehl, IEEE Trans. Nucl. Sci. **NS-24**, 1648 (1977).
[16]J.L. Adamski, P.S.P. Wei, J.R. Beymer, R.L. Gray, and R.L. Copeland, Ref. 12, p. 497.
[17]J.W. Poukey and N. Rostoker, Plasma Phys. **13**, 897 (1971).
[18]O. Zucker, J. Wyatt, H. Sahlin, J.S. Luce, and B. Freeman, Proc. 2nd Int. Topical Conf. on Collective Methods of Acceleration, Laguna Beach, Calif., 1978 (unpublished).
[19]J.S. Luce, W.H. Bostick, and V. Nardi, Proc. Conf. on Plasma Heating, Verona, Italy, 1976 (unpublished).
[20]W.W. Destler, H. Kim, G.T. Zorn, and R.F. Hoeberling, Ref. 18.
[21]C.L. Olson, Ref. 10, p. 312.
[22]C.L. Olson, G.W. Kuswa, D.W. Swain, and J.W. Poukey, Proc. 2nd Symposium on Ion Sources and Formation of Ion Beams, Berkeley, Calif., 1974, p. III-3-1 (unpublished).
[23]V.S. Voronin, Yu.T. Zozulya, and A.N. Lebedev, Zh. Tekh. Fiz. **42**, 546 (1972) [Sov. Phys.-Tech. Phys. **17**, 432 (1972)].
[24]H.R. Jory and A.W. Trivelpiece, J. Appl. Phys. **40**, 3924 (1969).